www.maajournal.com

Mediterranean Archaeology and Archaeometry
Vol. 20, No 2, (2020), pp. 45-65
Open Access. Online & Print.

DOI: 10.5281/zenodo.3746942

MULTISCIENTIFIC ANALYTICAL APPROACH OF POLYCHROME GRECO-ROMAN PALETTE APPLIED ON A WOODEN MODEL NAOS: CASE STUDY

Medhat Abdallah*[1], Ahmed Abdrabou[2] and Hussein M. Kamal[3]

[1]Director of conservation, Saqqara storerooms
Wood Lab-Conservation Centre, The Grand Egyptian Museum, Cairo, Egypt
[2]Conservation Centre, The Grand Egyptian Museum, Cairo, Egypt

Received: 10/10/2019
Accepted: 03/04/2020
** Corresponding author: Medhat Abd allah (Medhat.a.abdelhamid@gmail.com)*

ABSTRACT

In this paper, a nondestructive multiscientific analytical technique approach was used in order to map and identify how the palette of pigments and the painting techniques used by ancient Egyptian artisans on wooden substrate, since old kingdom to the New Kingdom (2575-1070BC), have been developed and enriched in the Greco-Roman period (30 BC-AD 311).

For first time the multiscientific combined methodology is applied on a polychrome naos dates back to Greco-Roman period, and shed light on the degradation of some of this pigments. The painted materials layered on the wood surface were analyzed by several scientific methods; optical microscopy (OM), technical photography, X-ray fluorescence (XRF), X-ray diffraction (XRD), SEM, FTIR-ATR, Imaging techniques (IR, VIL, UV). The application of technical photography provided useful information about the spatial distribution of the surviving original pigments, in particular visible-induced luminescence, which played an important role to recognize spatial distribution of areas containing Egyptian blue, Ultra violet induced luminescence emphasize using two kind of white pigments.

The results obtained by this technique indicate that the brown color is obtained by using a mixture of black (ivory black) and red pigment (cinnabar) which considered a new developing for the methods commonly used for obtaining brown color. Besides using lead white in the areas of bright white as overpaint for dull white substrate, using mixture of Egyptian blue and earthy green to obtain bluish green, the use of Huntite as an underpaint layer over the preparation layer in the yellow pigment area is due to its bright white color that reflects light from the paint and gives it more color saturation and brightening and yellow pigment is orpiment, however examination indicate that areas of degraded orpiment appear off-white.

KEYWORDS: Polychrome; Greco-Roman, Technical photography, Cinnabar, XRF, XRD, UV, Optical Microscopy, Egyptian Blue, White Lead

1. INTRODUCTION

In ancient Egypt pigments were widely used for the decoration of both large-scale monuments and small objects. The pigments of the "Pharaonic palette" (2575-1070 BC) consisted mainly of natural minerals (e.g. calcium carbonate and sulphate, iron ores, basic copper carbonate) whose ores were widespread in Ancient Egypt. By the Greco-Roman period (30 BC-AD 311) new and interested pigments were introduced to the Egyptian palette that includes: lead white, cinnabar (mercury sulphide) in addition to the earthy green (a mixture of celadonite and glauconite). (Lucas et al, 1989; Lee et al, 2000; Welcomme et al, 2006; Abdel-Ghani, 2009; Waltom,et al,2009).

A number of relatively recent studies have been published in the last years covering from the Old Kingdom up to the Greco-Roman Period; a multiscientific analysis approach combining imaging and spectroscopic techniques was applied for the study of some ancient Egyptian polychrome artefacts, as a result of these studies, the presence of some pigments has been confirmed; other pigments were established to much earlier dates as it thought and pigments which were originally thought to be degradation products have been added to the main palette, (Scott et al, 2004; Hühnerfuβ et al., 2006; Calza et al, 2011; Bracci et al, 2015; Cosentino, 2015; Abdrabou et al, 2017; Abdrabou et al, 2018; Pigment Catalogue, 2019; Afifi et al., 2020).

In this paper, we demonstrate the ability of combining imaging techniques and portable XRF as a very efficient and non-destructive method for analyzing the painted layers, for first time in a wooden naos. A complementary technique such as X-ray diffraction was used in some cases to confirm the identity of certain pigments. Wood, textile identification and isolating molts of insects were, also, detected on the studied object.

The Studied object

The wooden naos was built to hold the mummified body of the falcon; the falcon was believed to be a sacred bird in ancient Egypt. Horus, the son of Isis and Osiris, was identified also with the deities Ra, Montu, and Sokar. Naos has a form of a temple with a projecting cornice, the walls taper as they rise and are covered by different colors, with a small statue of falcon fixed on the naos's lid.

The studied object is a polychrome wooden naos (Fig. 1), which dates back to the Greco-Roman period (30 BC-AD 311), lined with stucco and painted with polychrome pigments (Blue, Green, Red, Brown, Black, White, Yellow and Gold leaf). Four scenes depicted the deceased honor the ancient Egyptian Gods and Goddesses on four sides' of naos. Remains of fabrics and insects' molts were founded inside the naos. A small painted wooden falcon with gilded face, two long plumes and a gilded sun disk on its head, represents the sun god Ra, is fixed on the cover of the naos, which might indicate that it had been used to house a mummy of a falcon. This naos is stored in the Grand Egyptian museum storerooms under registration No. GEM_No. 34381.

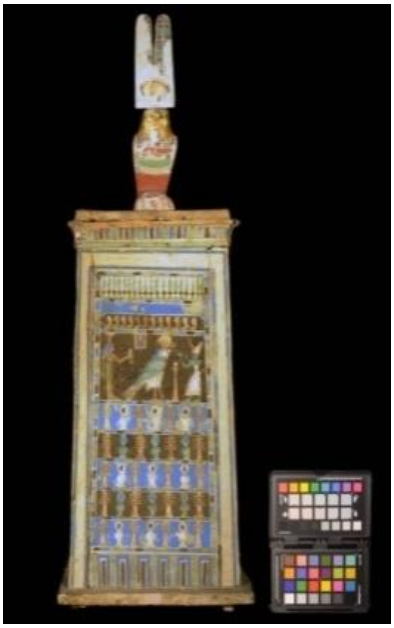

Figure 1. General view of the naos with colour checker (Dimensions: H. 69.5 cm, W. 26.5 cm, L. 27 cm)

2. MATERIALS AND METHODS

Methodology and sampling

This study based on the data obtained by visual examination with naked eye and optical microscopy, areas of represented painted and preparation layers were carefully chosen for investigation. X-ray florescence spectrometry (XRF) spots analyses were performed directly on the pigments and preparation layer, Micro fallen samples of some painted and preparation layers (preparation layer, red, blue and bluish green) were analyzed using X-ray diffraction (XRD) and Fourier transform infrared spectroscopy (FTIR), for studying the stratigraphic structure of gilded gesso a cross-section was prepared using epoxy resin (Epofix, Struers) and photographed by optical microscopy (OM) and scanning electron microscope (SEM).(see review in Bratitsi et al., 2019).

In order to identify the wood species, the naos was sampled at four points. Two samples were obtained from the wooden planks, while third sample was obtained from an original wooden dowel and the fourth sample was obtained from a wooden slit at the bottom of the naos. Wood samples were cut into the three principal anatomical directions: trans-

verse, tangential longitudinal and radial longitudinal. These three thin sections were then mounted on glass slides to be observed under transmitted light using Optika Microscopy (Italy) equipped with an Optika B9 Digital Camera (see Afifi et al., 2019; Medhat et al., 2018).

For identification of insects' molts, molts were carefully isolated and mounted on slide glasses to be observed under reflected light using stereo microscopy, Zeiss Stero DV 20, equipped with Axio Cam MRC5. In order to identify the Fibers of remains fabrics, fibers were mounted on glass microscope slides, while unstained fibers were examined easily with no preparation, provided fibers were mounted in a medium of lower refractive index. Plant fibers typically have a refractive index of 1.53–1.55, so glycerol, which has a refractive index of 1.47, has been used for mounting the fibers on glass slide, viewed under the microscope in transmitted light (Donaldson, 2009).

The observation and description of anatomical features allowed the identification of the taxon of wood species, molts and type of fibers through comparison with the description available in textbooks, atlases and database.

X-Ray Fluorescence (XRF)

X-Ray fluorescence measurements were carried out with portable system, thermo scientific Niton XL3t analyzer includes X-ray tube with Ag anode, 50kV and 0-200μA max, both metal and mining modes were employed and spot measurements with a diameter of 3 were made, duration of exposure was 60 second.

X-ray Diffraction (XRD)

X-ray diffraction measurements were carried out using X-ray Diffractometer System PW3040–Analytical Equipment–PANalytical pro model, Cu-target tube and Ni filter at 40kV and 30MA. X'Pert-Highscore software was used for identifying.

Fourier Transformed Infrared Spectroscopy (FTIR)

Fourier transform infrared spectroscopy was done by using FTIR spectrometer (VERTEX 70, Bruker) equipped with An attenuated total reflection (ATR) technique, spectrum in the range 4000-400 cm-1, spectra were measured at a resolution of 4cm-1 and 16 scans were recorded per sample.

Technical photography (TP)

Technical images in different spectral ranges (from 360 to about 1000 nm) were recorded using a Nikon D90 DSLR (CMOS sensor) digital camera modified for "full spectrum" and fitted with a Nikon Nikkor 18-70mm f/1:3.5G AF lens. The camera was operated in fully manual mode and was tethered to a computer to allow sharp focusing in non-visible modes (IR and UV) using live view mode. The camera has been calibrated with the X-rite Color Checker Passport and its bundled software to create a camera profile for Adobe Camera Raw. The filters and radiation sources used for imaging techniques were summarized in table 1.

Table 1. The filters and radiation sources used for imaging techniques

Imaging techniques	Filters	Radiation sources
Visible (VIS)	X-Nite CCI	white LEDs lambs
UV-induced visible luminescence (UVL)	UV/ IR Baader filter + X-Nite CCI	UV LEDs lambs
UV-reflected (UVR)	A Schneider W 403 + X-NiteCC1	UV LEDs lambs
Visible-induced infrared luminescence (VIL)	a Schott RG840 cut-on filter	white LEDs lambs
Infrared (IR)	a Schott RG840 cut-on filter	IR LEDs lambs
Infrared false color (IRFC)	made by digitally editing the VIS and IR images by adobe Photoshop	

The ultraviolet-induced visible luminescence technique is particularly useful in locating the presence of organic materials and colorants (lake pigments, ancient binders or varnishes) as well as many modern retouching or coating materials (Grant, 2000; Verri et al, 2008). Moreover, some inorganic materials also show luminescence properties that can give an indication of the identity of the pigments (Garcia – Moreno et al, 2013; Stuart, 2007). In the case of visible-induced infrared luminescence imaging (VIL), this technique was used to reveal the presence of Egyptian blue pigment that shows photo-induced luminescence properties in the infrared range (Verri et al, 2010; Verri et al, 2010; Verri et al, 2017), in the

VIL images, Egyptian blue pigment shows up as bright white areas against a dark background. Infrared (IR) imaging technique is useful in revealing the presence of any preparatory drawings or carbon-based pigment (Passmore et al, 2010 ; Abdrabou et al, 2018).

Raking light

Raking light is a technique in which a painting is illuminated from one side only, at an oblique angle in relation to its surface. Raking light is used to reveal a painting's surface texture. Raised paint surfaces facing the light are illuminated, while those facing away create shadows. The increased appearance of paint texture can easily be seen, photographed or recorded digitally. Conservators use raking light to judge aspects of the condition of a painting (Raking light, 2019).

3. RESULTS AND DISCUSSION

Wood Identification

The microscopic images of the anatomical characteristics of wood thin sections show that, the planks of polychrome naos are made of local hardwood sycamore fig [*ficus sycamorus* L. (Moraceae)] (Fig. 2), while the dowels and small wood slit at the bottom of the naos are made of another indigenous hardwood, tamarisk (*tamarix* sp.) (Fig. 3) (IAWA Committee, 1989 ; Hoadley, 1990; Cartwright et al 2011; Crivellaro et al, 2018, Tamarix sp., 2019).

Fig trees grew along the banks of the Nile; fig wood is of medium quality, pale, fibrous, coarse, light and easy to carve, susceptible to insect attack but if the wood heavily painted this drawback can mitigate to a relative degree. Tamarisk is occasionally mentioned in the ancient texts from old kingdom onward. Tamarisk is coarse and denser than fig wood; tamarisk wood could be used for loose tongues and dowels in the internal construction of wooden artifacts. Religiously the ancient Egyptian thought that; the sycamore tree symbolized the goddesses Isis and eventually Hathor, after the assimilation of Isis to *Hathor*. The tamarisk tree represented the god Osiris (Lucas et al, 1989; Gale et al, 2000; Daines, 2008; Dawson et al, 2016;).

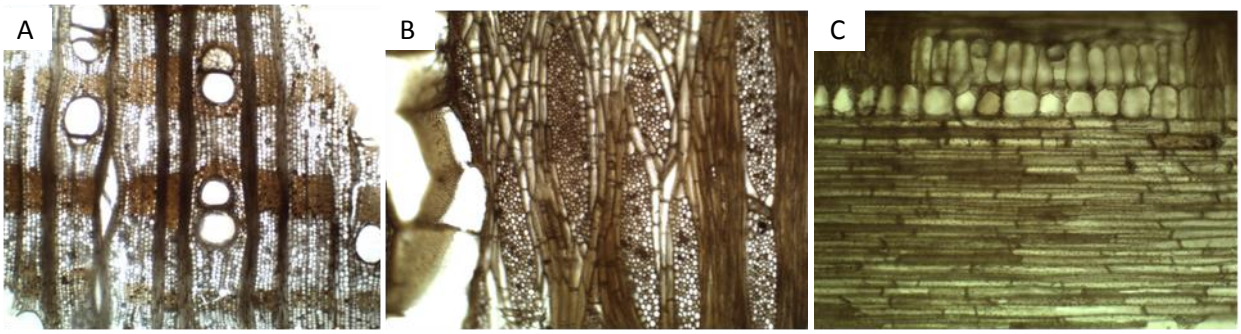

Figure 2. The anatomical characteristics of Ficus sycomorus by OM in transmitted light: A - Transverse section (TS) showing vessels solitary or in radial multiples of 2 to 4 and banded axial parenchyma with most bands greater than four seriate; B - Tangential section (TLS) showing rays of two distinct sizes, larger rays commonly 4 to 12 seriate; laticifers were observed in rays; C - Radial section (RLS) showing body ray cells procumbent with one to 4 rows of upright and square marginal cells.

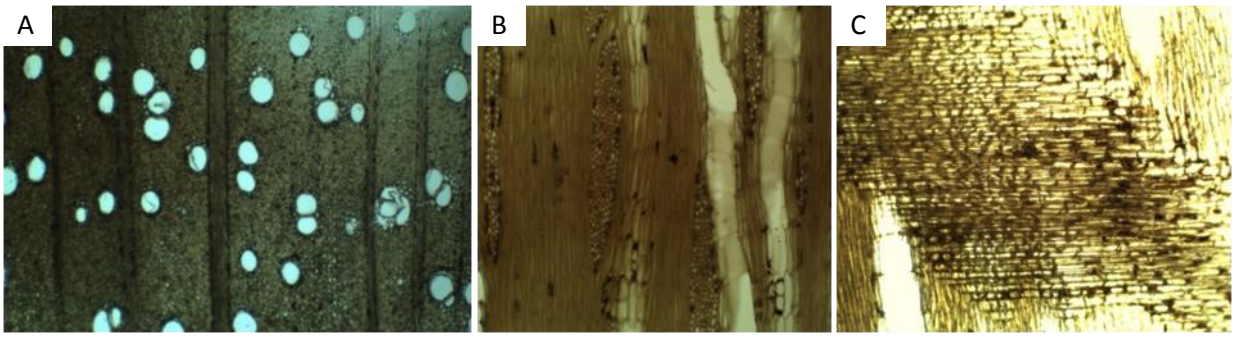

Figure 3. The anatomical characteristics of Tamarix sp. by OM in transmitted light: A. Transverse section(TS) showing wood semi-ring-porous to diffuse, vessels solitary and in small clusters and Axial parenchyma present in vasicentric or confluent distribution; B. Tangential section(TLS) showing multiseriate rays commonly 5–20 cells in width; simple perforation plates and inter vessel pits alternate. C. Radial section (RLS) showing heterocellular rays with procumbent, square and upright cells mixed throughout the ray.

Insect Identification

Molts of two larva were isolated from the naos, according to the diagnostic morphology the species of the first larvae molt (Fig. 4a) is black carpet beetle (*attagenus unicolor*) characterized by brown to tan, carrot shaped with long tufts of hairs extending from the abdomen, reach to 8 -13 mm long. the second larva molt (Fig. 4b) is identified as varied carpet beetle (*anthrenus verbasci*) characterized by alternating light and dark brown transverse stripes, covered with dense tufts of hair that extend upright if disturbed and reach to 4 mm long (Peacock, 1993; National park service 2008; Identification of Carpet beetles 2019; Identification of museum pests, 2019; Abdel-Maksoud et al., 2019).

Figure 4. Molts of two larva isolated from the naos: (A) Black carpet beetle (attagenus unicolor) (B) varied carpet beetle (anthrenus verbasci).

Textile Identification

Fabrics of textile have been used in ancient Egypt to wrap the Gods, Goddesses and royal statues positioned in naoses; residual of this fabrics have been found inside the naos (Fig. 5A) and impression of this fabric on the painted layer of Horus statue has been detected by optical microscopy (OM) (Fig. 5B), which suggest that this fabrics have been used to wrap the falcon *Horus*.

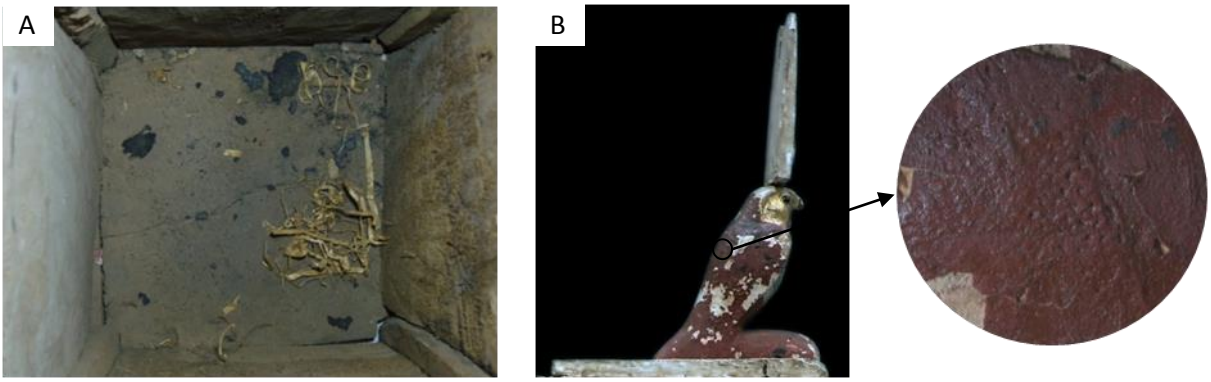

Figure 5. (A) Remains of textile inside the naos. (B) Impression of textile on painted layer.

Optical examination (Fig. 6) of longitudinal features by (OM) for remains of textile showed that single fibers or ultimate have nodes at intervals along fibre length in the form of I, V, or X, similar to the appearance of bamboo, irregular width, interior central lumen is quite small, typically less than half the full width of the fibre, often seen as a bundle of fibers tightly packed in the lengthwise direction, rather than as individual fibres (Florian, 1990; Canadian Conservation Institute (CCI) Notes, 2019).

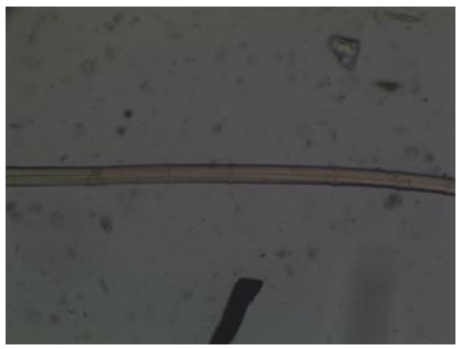

Figure 6. The structure of linen fiber shows nodes at intervals along fibre length, similar to the appearance of bamboo (Magnification 400X.).

Investigation of pigments and preparation layer

The chromatic palette applied on this naos includes white, red, blue, green, yellow, brown and black. Addition to gilding layer applied on white preparation layer; (Fig. 7) and table (2) locates and summarizes the XRF analysis results of pigments and preparation layers.

Table 2. The results of X-ray fluorescence (XRF) for the pigments and preparation layer

Spot	Color	elements
1	The preparation layer (the body of naos)	**Ca**, Si, Fe, Sr
2	The preparation layer (the statuette of *Horus*)	**Ca**, **Si**, S, Cl, K, Sr, Fe, As
3	White	**Pb**, **Cl, S, As, P, Ca, Fe, Si**, Ni, Al, Co
4	Red	**Ca**, **Fe**, **S**, **Si**, Cl, As, Sr, K, Al, Cr, V, Ti
5	Blue	**Cu**, **Ca**, **Si**, Fe, K, Cl, S, As, Pb, Ti
6	Green (light) (Chest of Horus statue (A))	**Ca**, **Cu**, **Cl**, **S**, Si, **As**, Fe, K, P, Sr,
	Green (light) (left feather of Horus statue (B))	**Ca**, **Cu**, **S**, **Cl**, Si, P, K, Fe, As, Sr, Pb
7	Green (bluish) (back of Horus statue (A))	**Ca**, **Si**, **Mg**, **Cu**, **S**, **Cl**, **Al**, **Fe**, **K**, Ti, Pb, As, Sr
	Green (bluish) (depicted of Horus on naos's body (B))	**Ca**, **Si**, **Mg**, **Cl, Cu**, **S**, **Al**, **Fe**, **K**, Pb, Ti, **As**, Sr
8	Yellow	**Ca**, **S**, **As**, **Mg**, Si, Cl, Fe, K, W, Sr, Pb
9	Brown	**Ca**, **Hg**, **S**, **Si**, **P**, **Cl**, **Fe**, Al, K, Ti, As, Au, zn, Sr
10	Black	**Pb, S, Ca, Cl, As, Si, P**, Al, Fe, Mn, Cu, Co
11	Gilding layer	**Au**

* *Bold element indicates correlation with the main preparation layer and pigments minerals and relatively high percentage of those elements.*

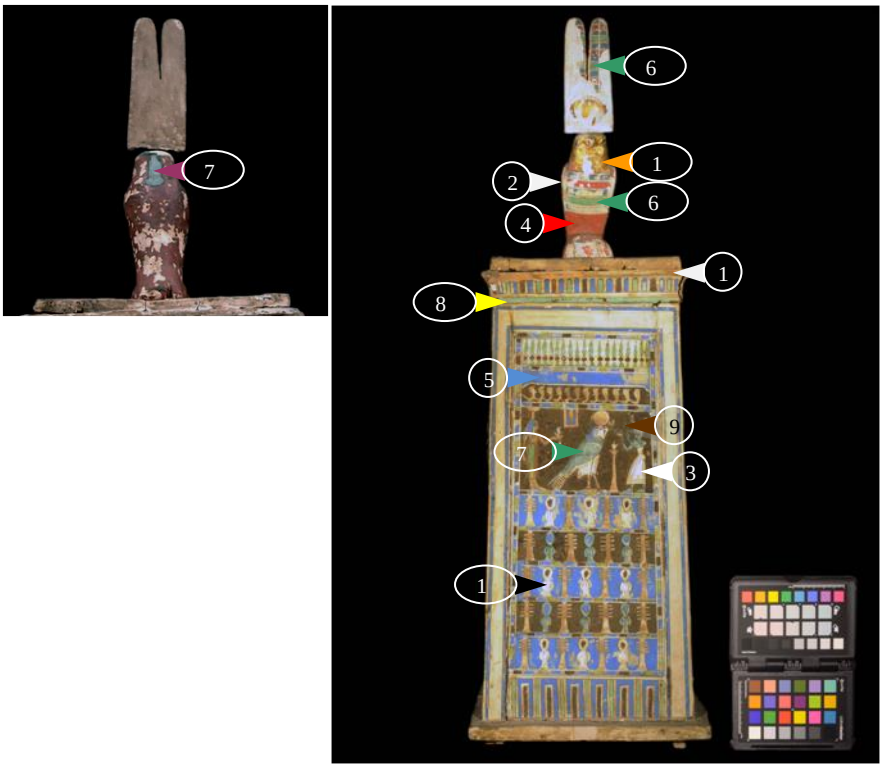

Figure 7. Areas of represented painted and preparation layers were carefully chosen for investigation. (Spots listed in Table 2 indicated by coloured head arrows).

The preparation layer and white pigments

The preparation layer

Investigation of the preparation layer by (OM), (XRF) and (XRD) show that calcium carbonate ($CaCO_3$) was used as a preparation layer for the naos and the statuette of Horus, while calcium sulphate ($CaSO_4$ $2H_2O$) have been used as filler between the bottom wooden slits of the naos.

- **Calcium Carbonate (body of naos)**

The XRF spectrum of the preparation layer applied on the body of naos indicate the presence of Calcium (Ca) as a major element; Traces of silica (Si), iron (Fe), strontium (Sr) were also detected. This result suggests that the preparation layer is calcium carbonate $CaCO_3$; while (Si) element may be due to silicon dioxide SiO_2. The XRD analysis (Fig. 8a) confirmed that the preparation layer of naos's body is composed of calcium carbonate ($CaCO_3$) and quartz (SiO_2).

- **Calcium Carbonate (statuette of Horus)**

The XRF spectrum of the preparation layer applied on the statuette of *Horus* indicate the presence of Ca (Calcium) as a major element; and traces of silica (Si), sulfur (S), arsenic (As), iron (Fe), chlorine (Cl), potassium (K) and strontium (Sr) were also detected. This result suggests that the preparation layer is of calcium carbonate. The XRD analysis (Fig. 13) confirmed that the preparation layer of the statuette of *Horus* is calcium carbonate ($CaCO_3$), and quartz (SiO_2).

- **Calcium sulphate (filler material)**

Investigation of the chemical compound of filling material (founded at the bottom of the basemen) by (XRD) (Fig. 8b) confirmed that calcium sulphate $CaSO_4.2H_2O$ have been used for filling gaps and separation between panels of the basement of naos's body.

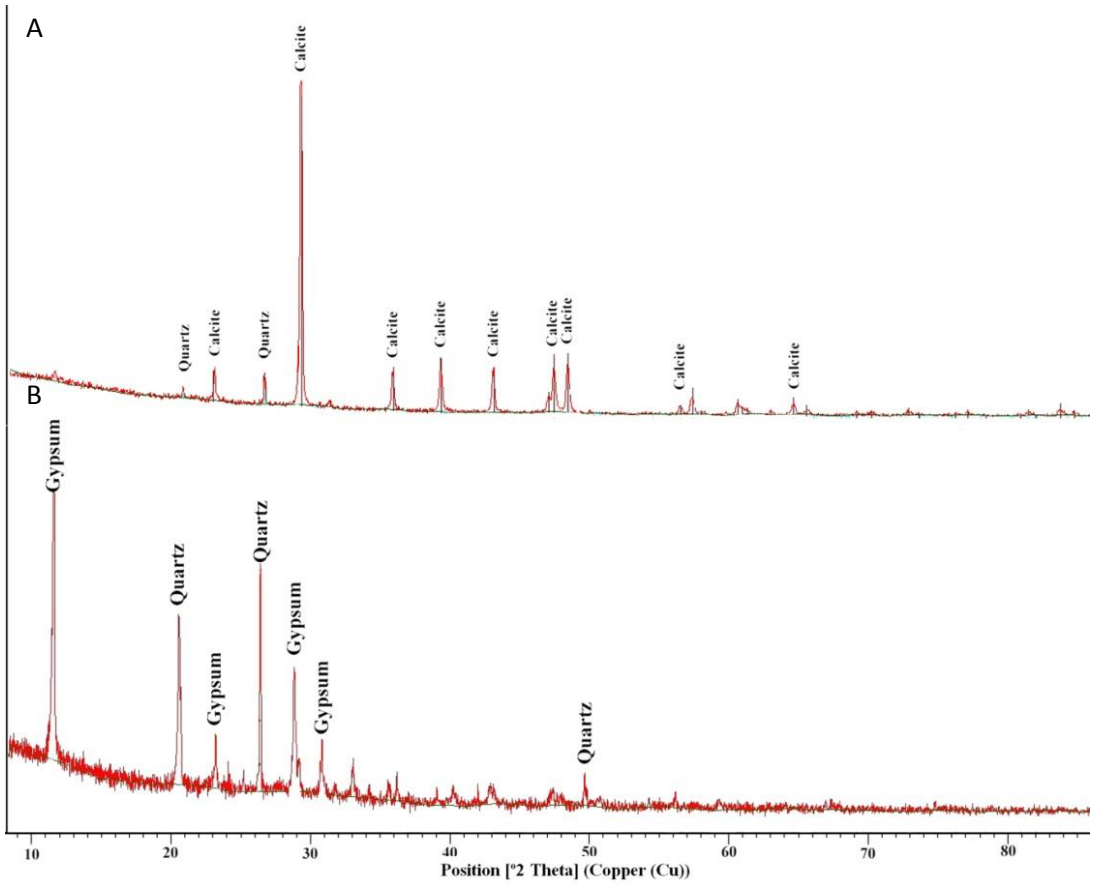

Figure 8. The XRD spectrums: (A) the preparation layer applied on the body of the naos. (B) The filling material.

White pigments

Visual and (OM) examination showed two types of whites have been applied by ancient Egyptian artisans, the microscopic examination of these white painted layers shows dull, fine and homogeneous morphology of the surface for one white pigment used as preparation layer and white layer (Fig. 9a), while the other white layer is fine, homogenous, bright (Fig. 9b) and founded in a specific area al-

lowed us to suggest that this white have been used as corrections by the master of the workshop antiquities or as interventions by other artisan in antiquity.

- **Dull white**

It is clear from the XRF spectrum (table 2) that the calcium (Ca) is the major element, besides, other minor detected elements, and this result provides a strong evidence of utilizing calcite ($CaCO_3$) as a white pigment. Applying XRD confirmed this result (Figure 8a).

- **Warm masstone white**

XRF analysis of warm white proved the presence of calcium (Ca), iron (Fe), silicon (Si), (Cl) chlorine, (P) phosphorus, (S) sulfur, (As) Arsenic, with traces of Cobalt (Co), manganese (Mn), aluminum (Al), nickel (Ni) and high percentage of Lead (Pb) which suggest that the warm masstone white is corresponded to the mixture of two compounds: hydrocerussite $2PbCO_3 \cdot Pb(OH)_2$ and cerussite $PbCO_3$ in various proportions; it is more generally called "lead white" (Goltz et al, 2003; Pagès-Camagna et al, 2010). Areas of bright white pigment appeared yellowish in the ultraviolet-induced visible luminescence imaging (UVL) image while dull white is bluish (Fig. 10). This pigment, a white lead carbonate ($2PbCO_3 Pb(OH)$), is a foreign material, found in Greek and Roman polychrome. In fact, it has been intentionally synthesized since Greek times and has been used extensively for artistic and cosmetic purposes (Welcomme et al, 2006). Applying this pigment in a specified area suggest that the ancient Egyptian artisan has used this pigment for enhancing the saturation and brightening of white area by lead white, because the XRF analysis of the white pigment indicate it is mainly made of calcium carbonate.

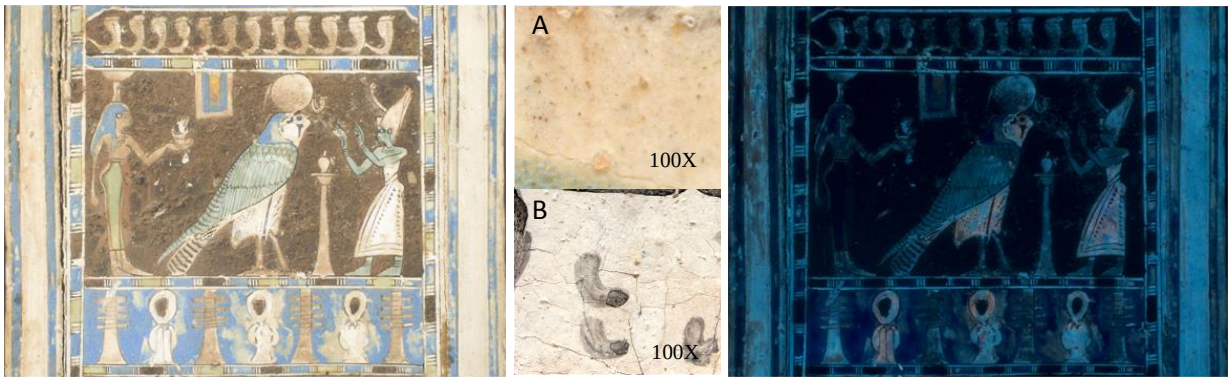

Figure 9. Two types of white pigments under optical microscopy show (A) Dull white pigment. (B) Warm white pigment.

Figure 10. Ultraviolet-induced visible luminescence imaging (UVL) showed dull white as bluish color and warm white as yellowish color.

Red pigment

The microscopic examination offered a clear and detailed view of the red painted layer showing the paint layered separated into many pieces distributed on the entire pigment surface with exfoliated colored layer in flakes shapes and dropping off in small flakes (Fig. 11 A-B). XRF analysis proved the high intensity of calcium (Ca), iron (Fe), sulfur (S) and silicon (Si) as main elements this result indicate that the red color is iron oxide (hematite) and the (Ca), sulfur (S) and silicon (Si) concentrations are due to the ground layer, besides traces of Chlorine (Cl), Arsenic (As), Strontium (Sr), potassium (K), aluminum (Al), chrome (Cr), vanadium (V), titanium (Ti). Areas of red pigment appeared darker in the ultraviolet - induced luminescence (UVL) image (Fig. 12), this is particularly evident on the red pigment of *Horus* (the falcon), which suggest that the red pigment is red ochre (colored by hematite, Fe_2O_3), consistent with the strong quenching properties of iron-based pigments (abdrabou et al, 2018).The principal red pigments in Egypt are of two main types, red iron oxide (hematite) and red ochre (hydrated iron oxide, perhaps partially dehydrated goethite) (Calza et al, 2007), Natural reds earths are of a different provenance, but their color is always given by the presence of hematite (Hradil et al, 2003). Microanalysis by XRD confirmed this result (Fig. 13). Red ochre was used from the 5th Dynasty till the Roman times, this Fe-based colors are longer lasting and light faster than others, and are sometimes of astonishing brilliance (Lee et al, 2000; Afifi, 2011). The presence of both (S) and (As) elements may suggest mixing a little portion of orpiment As_2S_3 with hematite to enhance the brightness of red color.

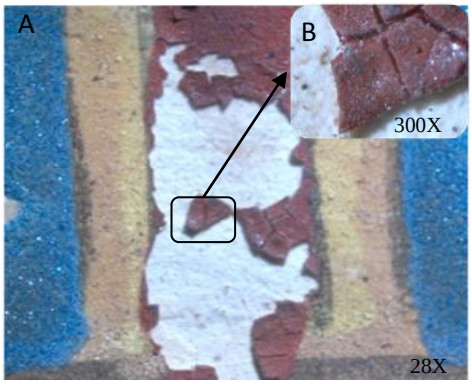

Figure 11. Red pigment under microscope (A) show lost red pigment (28X) (B) deep cracks and lifting.

Figure 12. Response of red hematite to technical photography: (A) Visible light (VIS). (B) Red pigment appeared darker in the Ultraviolet-induced visible luminescence imaging (UVL).

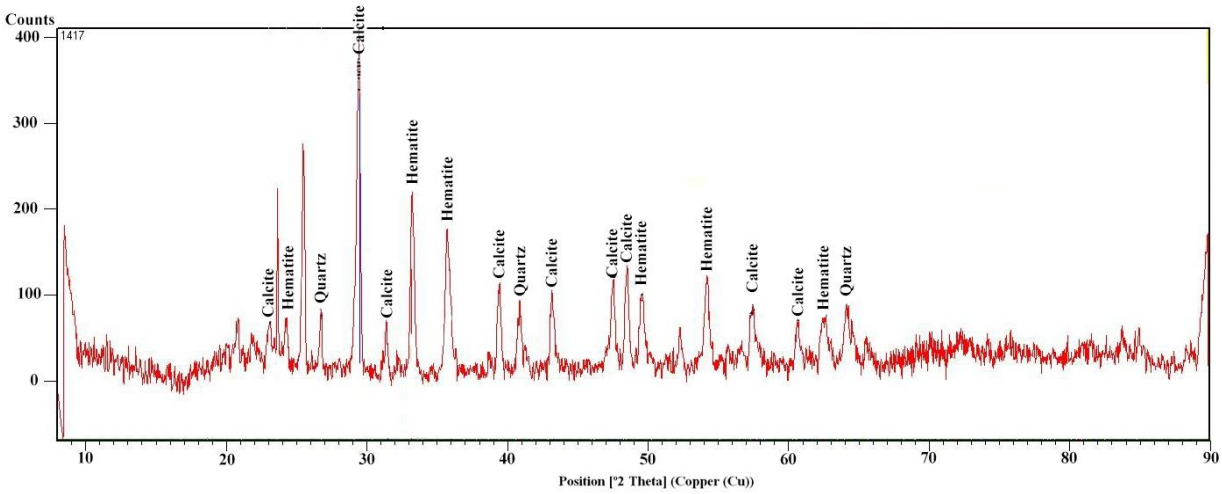

Figure 13. The XRD spectrum of the red pigment

Blue *pigment*

The microscopic examination of the blue painted layer (Fig. 14) shows coarse morphology of the surface and relatively homogeneous distribution of the grains. The microanalysis of the blue pigment, performed with XRF, shows that the high intensity of copper (Cu), calcium (Ca) and silicon (Si) the characteristic elements of Egyptian blue; addition to traces of iron (Fe), potassium (K), chlorine (Cl), sulfur (S), arsenic (As), lead (Pb), titanium (Ti). In the visible-induced infrared luminescence image (Fig. 15b); the blue color appeared as bright white, the luminescence of such areas could indicate the presence of Egyptian blue. In addition, infrared false color image (Fig. 15c) indicated that the areas painted with blue pigment appeared red, which confirm the presence of Egyptian blue. Numerous analysis of Egyptian blue has shown it to be a multiphase pigment containing cuprorivaite $CaCuSi_4O_{10}$ (Green, 2001); XRD analysis confirmed the presence of cuprorivaite the component responsible for the blue color (Fig. 16).

Egyptian Blue has been known since 2500 B.C. and is the oldest known synthetic pigment. It was prepared from natural materials and fine metal scraps by firing the mixtures at temperatures of about 800 ^oC (Abd El Aal, 2010). This pigment is found on every type of support and the large number of shades is created only by varying degrees of grinding, and not by mixing with other pigments: pale blue is obtained with tiny grains, less than 15 µm, whereas dark blue comes from 30 µm grains (Pagès-Camagna et al, 2010).

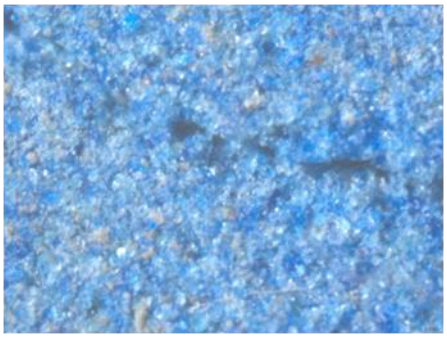

Figure 14. Blue pigment under microscope showed coarse and homogenous surface.

Figure 15. Technical photography of Egyptian Blue pigment A. Visible light (VIS) B. Visible induced Infrared luminescence (VIL) C. Infrared false color (IRFC)

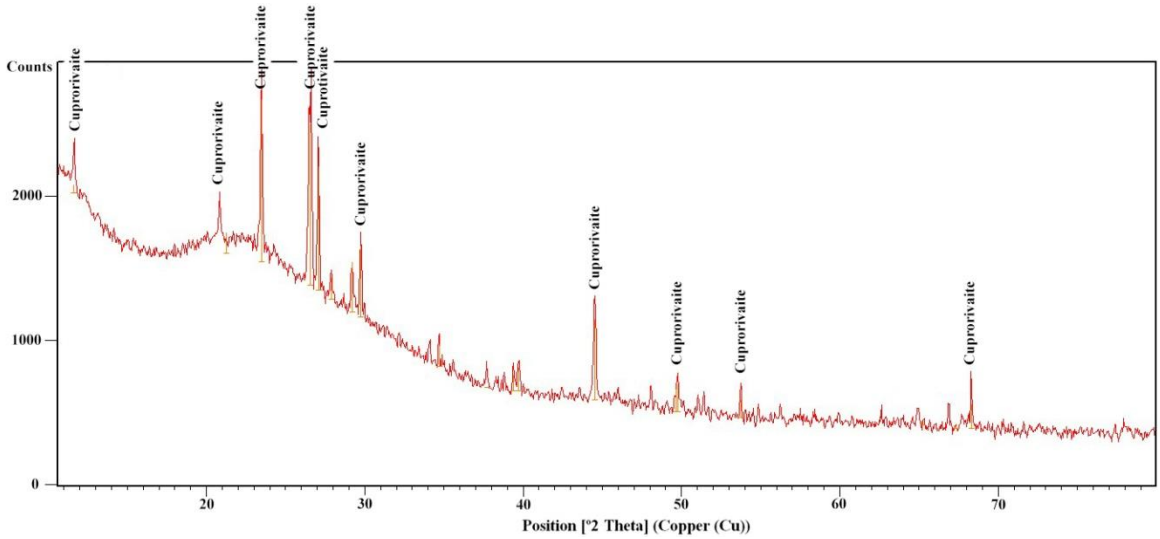

Figure 16. The XRD spectrum of the Blue pigment

Green pigments

Visual observation and microscopic examination show two types of green pigments applied on this naos light green and bluish green. Analysis by (XRF) and imaging by (MSI) gave us more information about these pigments.

Light green

The microscopic examination of the light green painted layer (Fig. 17) shows fine morphology of the surface, besides, micro cracks distributed on the entire pigment surface with exfoliated colored layer in flakes shapes and dropping off in small flakes. XRF analysis of light green pigments samples (A) and (B) show that the elements that presented the highest concentrations were: (Ca), (Cu), (S) and (Cl). The presence of (Cu) and (Cl) suggest the possibility of copper chlorides green pigments. In addition, the presence of (Ca) and (S) may be due to the gypsum $CaSO_4.2H_2O$. This may indicate that the light green in the sample (A) and (B) is a mixture of copper chlorides and gypsum. The green painted areas didn't show any UV fluorescence (Fig. 18a). This could be an indication of the presence of copper- based pigments, since they are known to quench fluores-

cence of surrounding media. Copper- based pigments are supported by the infrared image (Fig. 18b); where the green painted layers appear dark due to the high absorption properties of these pigments in the near infrared. VIL images (Fig. 18c) didn't show any luminescence of the green painted areas, therefore the hypothesis of a mixture of Egyptian blue and yellow pigments can be discarded (abdrabou et al, 2018).

Bluish green

The microscopic examination of the bluish green painted layer at the back of *Horus* statuette shows coarse morphology of the surface and relatively large crystals of blue pigment embedded in a matrix of fine green pigment grains (Fig. 19a); the whole sample was bluish green owing to the presence of other green mineralogical components. However, the use of mixture of blue pigment and green pigment has been reported in some works.

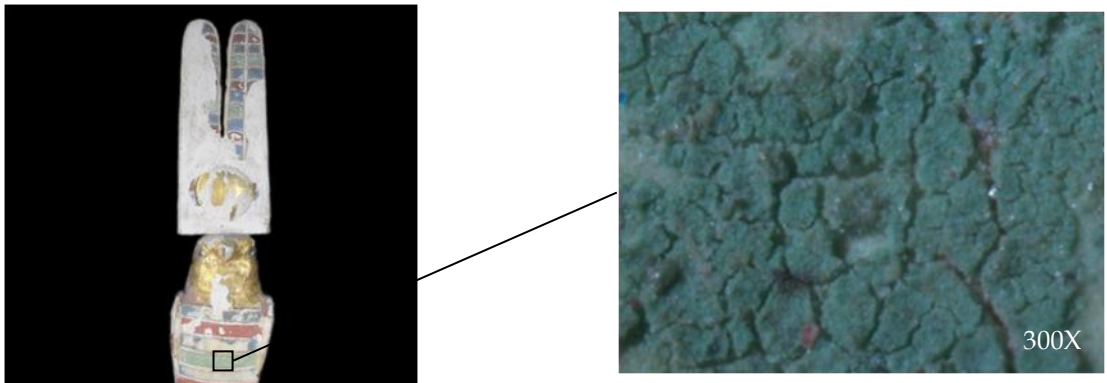

Figure 17. Green pigment (chest of Horus) under microscope showed fine morphology and microcracks.

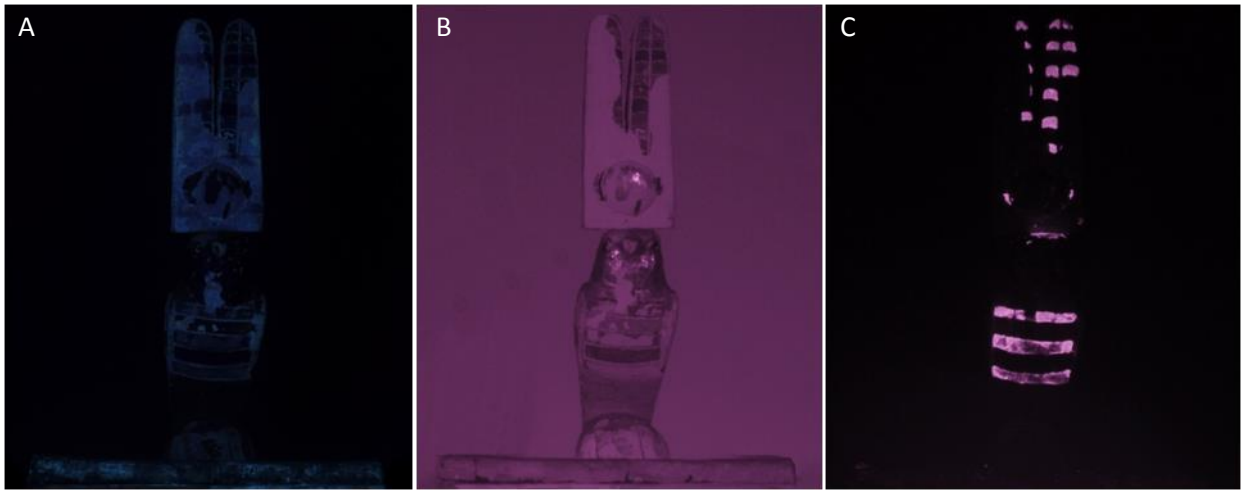

Figure 18. Technical photography of light green pigment: A. UV induced luminescence (VIL) B. Infrared (IR) C. Visible induced Infrared luminescence (VIL).

The results of the elemental analysis for two spots (A & B) of bluish green by (XRF) indicated the presence of (Ca), (Si), (Mg), (Cu), (Cl) and (S) as a major elements; and (Al), (Fe), and (K) as a secondary elements; besides, traces of (As), (Pb), (Ti) and (Sr). In this case, there are three possibilities of pigments, because XRF technique is able to determine only the elemental composition and not the chemical or geochemical forms of the analyzed samples, The presence of (Cu), (Si) and (Ca) suggests the possibility of Egyptian blue $CaCuSi_4O_{10}$, while the presence of (Mg), (Fe), (K) and (Al) suggests the possibility of green earth (a mixture of celadonite and glauconite), the color of celadonite has been described as earthy, dull, greygreen or bluish-green. The chemical composition of celadonite is approximately K [(Al, Fe^{3+}),(Fe^{2+}, Mg)] ($AlSi_3$, Si_4)$O_{10}(OH)_2$ (Mahmoud, et al, 2012), while the presence of chlorine (Cl) and copper (Cu) suggest the presence of low portion of copper chloride based green pigment. In the visible-induced infrared luminescence image (Fig. 19b and 20b), the blue color appeared as bright white. The

luminescence of such areas indicate the presence of Egyptian blue (Dyer et al, 2014), the presence of the Egyptian blue have been confirmed by (XRD) which detected quartz (SiO_2) and cuprorivaite ($CaCuSi_4O_{10}$) the main component of Egyptian blue (Fig. 21). These results suggest that the bluish green pigment may be a mixture of Egyptian blue, earthy green celadonite and portion of copper chloride based pigment. In many cases, Egyptian blue was added in small amounts to enhance the brilliance of other colors. The mixture of blue (Egyptian blue) and green (celadonite and glauconite) to form green pigments was reported by (Mazzocchin et al, 2003; Mazzocchin et al, 2003; Calza et al, 2007).

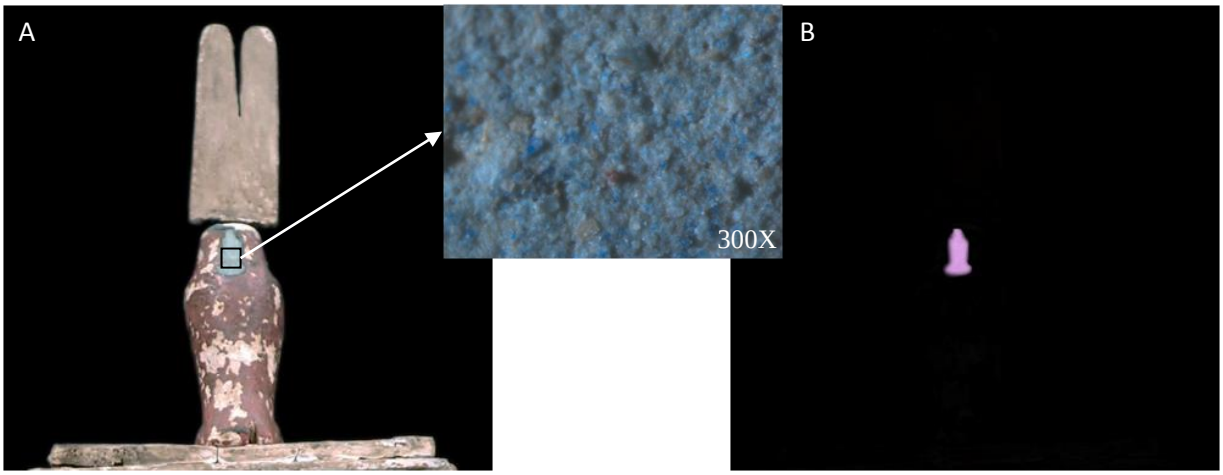

Figure 19. (A) Examination of bluish green pigment at the back of Horus's neck by (OM) shows blue grains embedded in green matrix. (B) Visible induced Infrared luminescence (VIL)

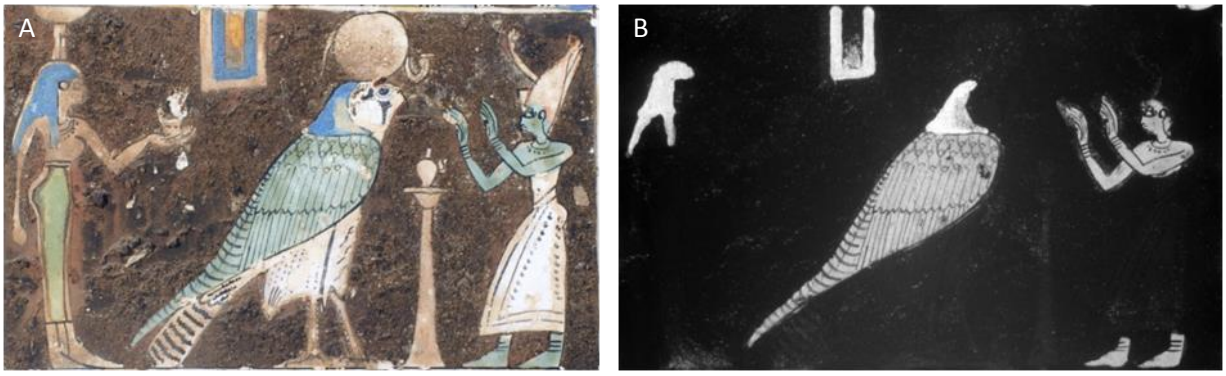

Figure 20. Technical photography of bluish green pigment: (A) Visible light photography (VIS) (B) Visible induced Infrared luminescence (VIL).

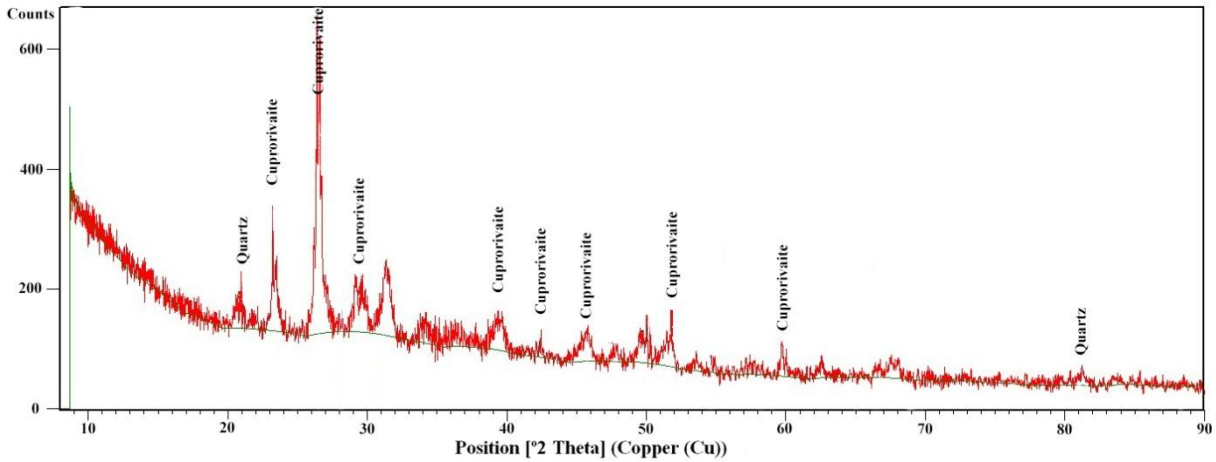

Figure 21. The XRD spectrum of the green bluish pigment

The Yellow pigment

The visual investigation by naked eye detected residuals of yellow pigment on the frames of the polychrome decorated pictorial areas. Microscopic examination of the yellow layer shows the homogenous of yellow pigment in some places (Fig. 22a) and fading of the color in others (Fig. 22b). The result of XRF analysis showed high percentage of calcium (Ca), sulfur (S), arsenic (As) and magnesium (Mg); besides, (Si), (Cl), (Fe) as a secondary elements and traces of (K), (W), (Sr), (Pb). This result provides a strong evidence for the presence of arsenic sulphides based yellow pigment may be orpiment As_2S_3. Calcium element is due to the preparation layer $CaCO_3$, while The (Mg) may be due to using huntite $CaCO_3.3MgCO_3$, Huntite appears at least as early as the Old kingdom and was still in use during the Roman period (Heywood, 2001), However, the use of Huntite as underpaint over the preparation layer in some instances has been reported in some studies (Heywood, 2001; Uda et al, 2000; McCarthy, 2001; Amber, 2004), The reason for its application as underpaint is due to its bright white color that reflects light from the paint and gives it more color saturation and brightening (Abdel-Ghani, 2009), while (Si) is due to silicon dioxide SiO_2.

Orpiment is a bright yellow with a stronger tonality, a natural arsenic sulphide, As_2S_3. Because of its color, orpiment was used instead of gold (Colinart, 2001). Orpiment, As_2S_3, has been reported to become off-white and fade when exposed to light for prolonged periods. This is due to oxidation of the arsenic sulphide, to produce white arsenolite As_2O_3. The rate of fading of orpiment depends on humidity as well as light level, the presence of UV light accelerates the rate of fading and high relative humidity has detrimental effects. There is a simultaneous loss of sulphur from the orpiment as it fades; this sulphur can subsequently react with adjacent pigments causing alteration in color (Green, 2001; David et al, 2001; Korenberg, 2008), This hypothesis can explain areas of degraded orpiment in the studied naos, which appear off-white; close examination of these areas reveals residual of yellow grains and the sparkle associated with the orpiment particles, this is due to the laminar structure of the mineral. The ultraviolet-induced luminescence (UVL) images showed evidence for the presence of adhesive or organic material as splashes by brushes (Fig. 23a,b).

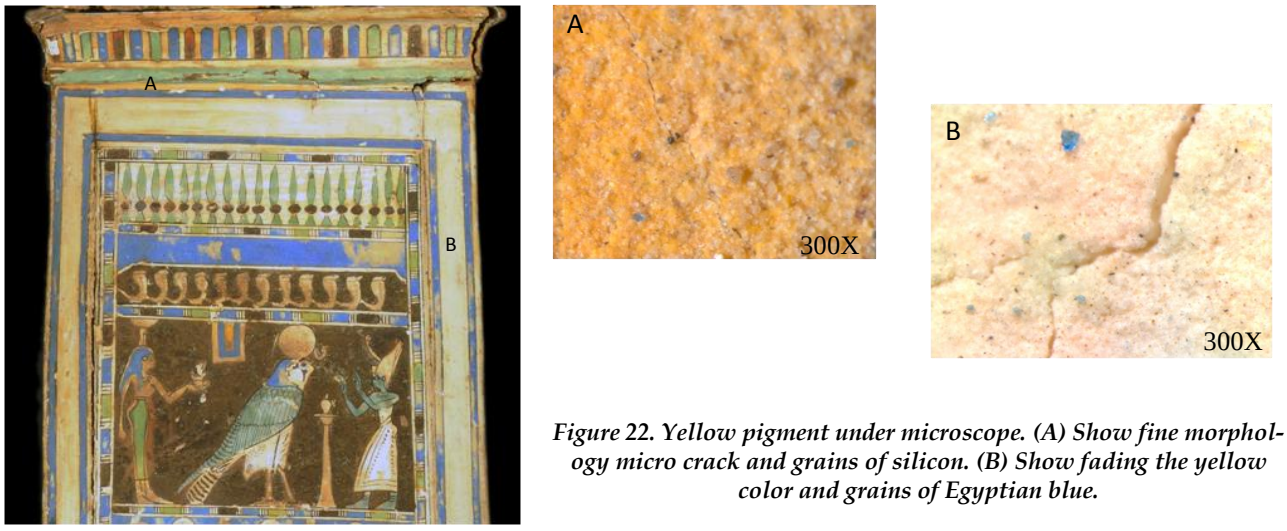

Figure 22. Yellow pigment under microscope. (A) Show fine morphology micro crack and grains of silicon. (B) Show fading the yellow color and grains of Egyptian blue.

Figure 23. Technical photography of painting medium: (A) visible light. (VIS) (B) The ultraviolet-induced luminescence (UVL) image showed evidence for the presence of adhesive or organic material as splashes by brushes.

The Brown pigment

Visual and microscopic examination of brown pigment layer shows a residual of red pigment mixed with a homogenous layer of black pigment and grains of sand and dust coat particularly the painted areas with brown pigment (Fig. 24a,b). The microanalysis elements by XRF indicate the presence of (Ca), (Hg), (S), (Si), (P), (Cl) as major elements and iron (Fe), aluminum (Al) and potassium (K) as secondary elements, traces of (Ti), (As), (Au), (Zn) and (Sr) are also detected. brown, in general, is a composite color, many studies states that iron oxide or ochre; black pigment with red ochre or a mixture of hematite with orpiment and carbon black were generally used for the color brown from fifth dynasty to roman period (Lucas et al, 1989; Lee et al, 2000; David et al, 2001; Calza et al, 2007). The high concentration of (Hg) and (S) suggest the presence of mercuric sulphide as a red color, while the presence of (Ca), (P) and (Cl) may be due to the carbon black (bone black), bone black (ivory black) is made from charring animal's bones. It contains about 10% carbon, 84% calcium phosphate (apatite) and 6% calcium carbonate together with organic matrix of collagen and lipids (Abdel-Ghani, 2009). Apatite is a group of phosphate minerals, usually referring to hydroxylapatite, fluorapatite and chlorapatite, with high concentrations of OH^-, F^- and Cl^- ions, respectively, in the crystal. The formula of the admixture of the three most common end members is written as $Ca_{10}(PO_4)_6(OH,F,Cl)_2$, and the crystal unit cell formulae of the individual minerals are written as $Ca_{10}(PO_4)_6(OH)_2$, $Ca_{10}(PO_4)_6F_2$ and $Ca_{10}(PO_4)_6Cl_2$ (Apatite, 2019).the presence of (Fe), (Al), (K) and (Ti) may be due to the sand and dust attracted to the brown color. The presence of titanium in the samples could be the result of the presence of ilmenite which is often found in Egyptian sand (Berry, 1999). The authors think that, in the brown pigment, the possibilities are a mixture of black (ivory black) and red pigment (cinnabar).

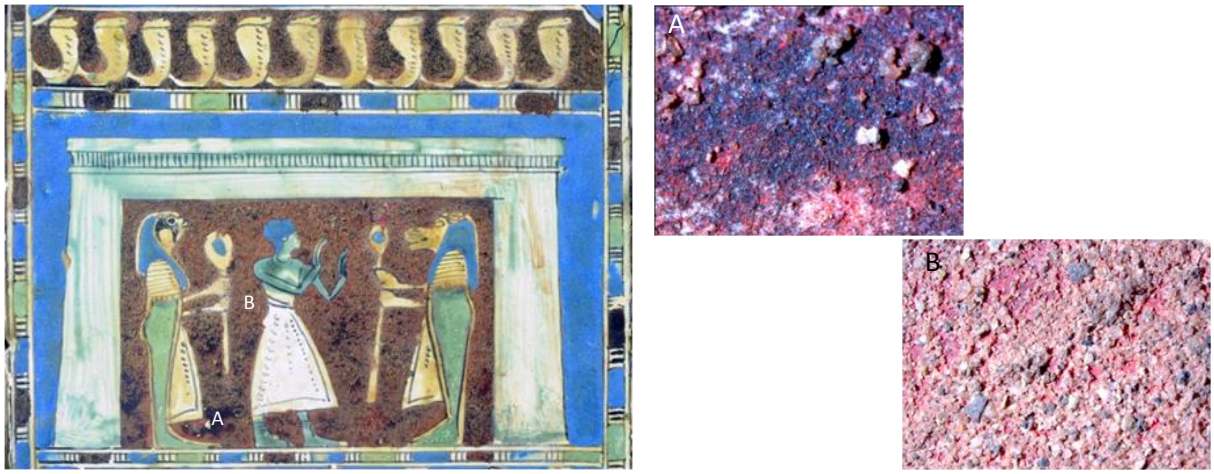

Figure 24. Brown pigment under microscope (A) Show fine morphology and spots of red color in a matrix of black color. (B) grains of sand and dust.

The Black pigment

The microscopic investigation of the black pigment indicated the homogeneous distribution of a fine-grained black and didn't show any fibrous structure (Fig. 25), so it is possible to exclude burnt vegetable origin of the black pigment. In XRF analysis, (Ca), (P) and (Cl) was detected. This result provides evidence for the presence of carbon obtained from the animal origin that is most likely bone black, which is one of the oldest pigments known to human, and was originally made by charring animal bones (Mahmoud, 2014). Areas of black pigments appear darker in the UVL image (Fig. 26a). This is particularly evident on the outlines of the naos, which may suggest that the black pigment is a carbon based black, consistent with the strong absorption properties of carbon (Abdrabou et al, 2017). In the IR image (Fig. 26b), hidden black outlines below the sand and dust layers appeared, while it was difficult to see the black outlines under the brown and blue painted layer. This is due to carbon black or copper-bearing pigments such as Egyptian blue are opaque under infrared emission and appear dark.

Figure 25. Black pigment under microscope showed homogeneous distribution of a fine-grained black.

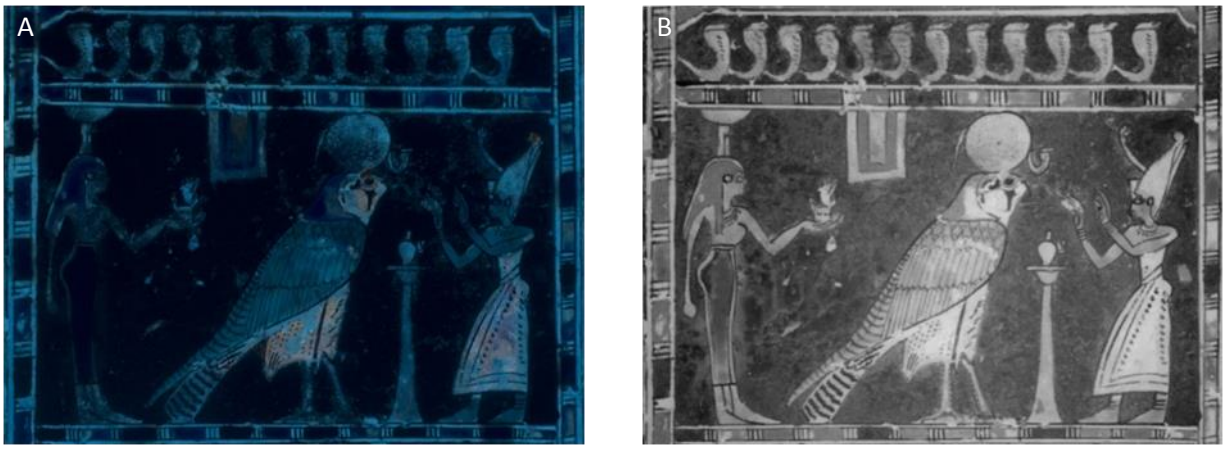

Figure 26. Technical photography of painting medium: (A) The ultraviolet-induced luminescence (UVL) image; black pigment appear darker, (B) IR image; hidden black outlines below the sand and dust layers appeared, and carbon black color is sharp.

The Gilding layer

Gilding is the technique whereby thin sheets of gold are applied over a firm support to achieve the rich appearance of solid gold. Many authors who studied gilding techniques agreed more or less to the following definitions for the description of the wide range of gold film thickness applied to various substrates (Lucas et al, 1989; Hatchfield et al, 1991; Rifai et al,2010; Darque-Ceretti et al, 2011; Abdrabou et al, 2018) :

- Gold sheet is a thick plate of gold obtained by the first hammering or rolling of the gold or gold alloy ingot.
- Gold foils have an intermediate thickness, more than about 10 µm, obtained by hammering or rolling the sheets.
- Gold leaves are obtained by beating. Their thickness is smaller than 10 µm and can be as low as 0.1 µm. They are not able to support their own mass and must be handled with a special knife blade or brush.

There is no evidence to suggest that the Egyptians made a terminological distinction between gold leaf and gold foil, but it is probable that especially skilled beaters were used to produce the former. The authors will use the term 'gold leaf' to describe the sample discussed in this paper (James, 1979).

The results obtained by XRF analysis (metal Mode) indicates that studied gold leaf is composed of pure gold (Au) 96.27% and traces of impurities includes Pb , Zn, Cu, Fe, Cr, and Ti elements. The studied sample has a distinctive dull, reddish-brown layer that was originally thought to be either a cuprite layer (due to selective corrosion of copper in the gold) or due to the presence of iron. Micrographs obtained by SEM shows that the gold leaf is applied on the ground layer, gold leaf ranges from 3.54 µm to 5.91 µm in thickness (Fig. 27a-b).

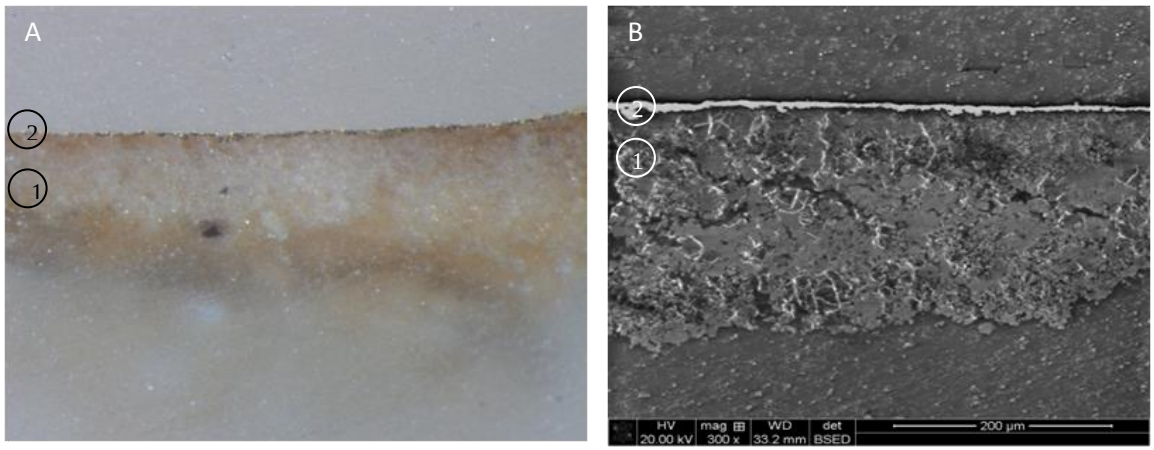

Figure 27. (A) Microscopic optical and environmental scanning electron microscope (ESEM) backscattered electrons mode, (B) micrographs showing the stratigraphic structure of the gilding for sample obtained from fallen fragments. (1) White preparation layer. (2) Gold leaf.

Raking light

Raking light (Fig. 28a,b) enhances the morphology of the relief decoration and reveals fine details includes; the direction and raised brushstrokes; raised Egyptian blue comparing to the other pigments, improving yellow pigment visibility; emphasize applying lead white over the already colored white area in particular areas. More importantly, from a conservation point of view, the raking light also reveals the sand accumulations on the paint surface. The cracks are virtually invisible in normal light.

Figure 28. Raking light: (A) normal light. (B) Raking light enhances the morphology and reveals fine details.

The preparation and painted layers binder

The binder used with the pigments and preparation layer was identified by FTIR analysis spectrum (Fig. 29) as animal glue, It is clear that the band at (3303 cm^{-1}) represents (OH) hydroxyl stretching due to intermolecular hydrogen bonding of the hydroxyl group and NH stretch of aliphatic primary amine (Wei, et al, 2016). The C─H stretching vibrations occurred in the region (2918 cm^{-1}) stretching of aliphatic groups. The band at (1635 cm^{-1}) (C ═ O stretching band) is assigned to amide I, the increasing or decreasing of C=O is dependent on the physical state of the sample, In the solid state the frequency of the vibration is slightly decreased, while the band at (1541 cm^{-1}) (C─N─H) is assigned to amide II (Derrick et al, 1999; Abdel-Maksoud et al, 2013). calcium carbonate can be detected by the presence of a strong band around 1417 cm^{-1}, characteristics of the C–O stretching mode of carbonate together with a narrow band around 873 cm^{-1} of the bending mode (Bosch et al, 2002; Al Dabbas et al, 2014).

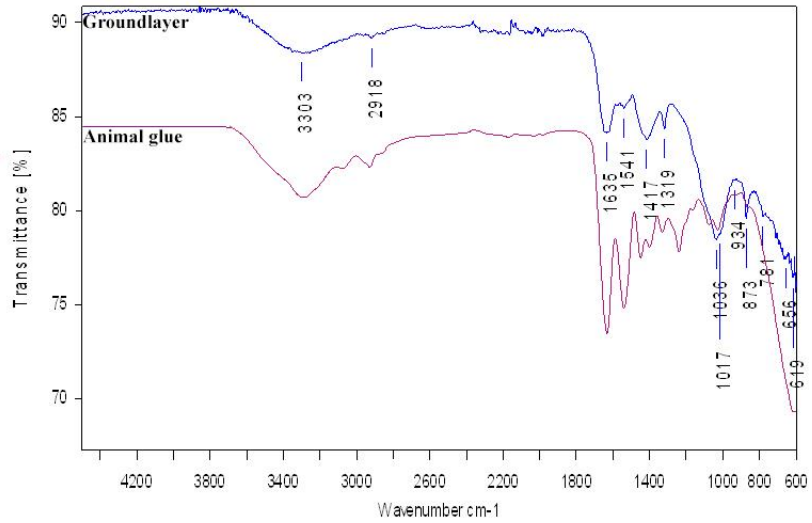

Figure 29. FTIR spectrum of the preparation and painted layers

CONCLUSION

The multi investigation approach includes optical microscopy (OM), X-ray fluorescence (XRF) and technical photography (TP), in addition to X-ray diffraction (XRD) as well as FTIR , imaging techniques, act as complementary techniques used to confirm the identity of certain pigments, characterized the structure and a common chromatic Greco-Roman palette applied on the studied polychrome wooden naos, which dates back to Greco-Roman period (30 BC-Ad 311). The results obtained indicate that the wood species that have been used for making the naos are indigenous wood sycamore fig for blanks and tamarisk for dowels, the roman polychrome palette applied on this naos include the preparation layer made of calcium carbonate $CaCO_3$ and numbers of pigments (white, red, blue, light green, bluish green, yellow, brown and black) analysis and examination reveal that the two white pigments were calcium carbonate and lead white cerussite $PbCO_3$, red is hematite Fe_2O_3 and blue is Egyptian blue cuproriviate $CaCuSi_4O_{10}$. The green pigments were identified as light green made of a mixture of copper chlorides based green mixed with white pigment calcium sulphate $CaSO_4.2H_2O$ while the bluish green is a mixture of earthy green $K[(Al, Fe^{3+}),(Fe^{2+}, Mg)](AlSi_3, Si_4)O_{10}(OH)_2$, Egyptian blue and a low portion of copper chlorides based green. Yellow pigment was identified as orpiment As_2S_3. The brown pigment was identified as a mixture of bone (ivory) black and cinnabar HgS. black carbon pigment was identified as bone (ivory) black. Because XRF technique is capable of determining only the elemental composition and not the chemical or geochemical form of the analyzed materials, it would be necessary to use an additional investigative technique in order to obtain an unambiguous identification of the pigments. Micrographs obtained by SEM shows that the gold leaf is applied on the white ground layer, gold leaf ranges from 3.54 μm to 5.91 μm in thickness.

ACKNOWLEDGEMENTS

The authors would like to thank our colleagues in analysis and examination labs for their cooperation and assistance.

REFERENCES

Abd El Aal, S. (2010) Identification of Painting Layers of Sennefer Tomb by Ion Beam Analysis, *Proceedings of the VIII International Conference ION 2010*, Kazimierz Dolny, Poland,Vol.120, No.1, pp. 144-148.

Abdel-Ghani, H. M. (2009) *A Multi-instrument Investigation of Pigments, Binders and Varnishes from Egyptian Paintings (AD 1300-1900): Molecular and Elemental Analysis Using Raman, GC-MS and SEM-EDX Techniques*. Unpublished Ph.D. Dissertation, Department of Archaeological Sciences, University of Bradford.

Abdel-Maksoud, G. and El-Amin, A. (2013) the investigation and conservation of a gazelle mummy from the late period in ancient Egypt, *Mediterranean Archaeology and Archaeometry*, Vol. 13, No 1, pp.45-67.

Abdrabou, A., Abdallah, M. and Kamal, H. M. (2017) Scientific investigation by technical photography, OM, ESEM, XRF, XRD and FTIR of an ancient Egyptian polychrome wooden coffin. *Conservar Património*, Vol. 26, pp. 51–63.

Abdrabou, A., Abdallah, Shaheen, I. and Kamal, H. M. (2018) Investigation of an ancient Egyptian polychrome wooden statuette by imaging and spectroscopy, *International journal of conservation Science*, Vol. 9, Issue 1, pp.39-54.

Abdrabou, A., El Hadidi, N., Hamed, S. and Abdallah, M. (2018) Multidisciplinary approach for the investigation and analysis of a gilded wooden bed of King Tutankhamun, *Journal of Archaeological Science*: *Reports* 21, pp.553–564.

Abdel-Maksoud, G, Abdelrahman Elamin, Afifi, F (2019) Evaluation of cedar wood oil (*cedrus libani a. rich*) for the control of common egyptian mummies' insect pest (*dermestes maculatus*). *SCIENTIFIC CULTURE*, Vol. 5, No. 2, pp. 31-36. DOI:10.5281/zenodo.2649503.

Accorsi, G., Verri, G., Bolognesi, M., Armaroli, N., Clementi, C., Miliani, C. and Romani, A. (2009) The exceptional near-infrared luminescence properties of cuprorivaite (Egyptian blue), *Chemical Communications*, Vol.23, The Royal Society of Chemistry, pp. 3392–3394.

Afifi,H.A.M, (2011) Analytical investigation of pigments, ground layer and media of cartonnage fragments from Greek Roman period, *Mediterranean Archaeology and Archaeometry*, Vol. 11, No.2, pp.91-98.

Afifi, H.A.M, Abd El-Kader, S, Hamed, M, Mohamedy, S, Dawod, M (2019) a dating approach of a refundable wooden egyptian coffin lid. *SCIENTIFIC CULTURE*, Vol. 5, No. 1, pp. 15-22. DOI: 10.5281/zenodo.1451900

Afifi, H.A.M, Rushdya Rabee Ali Hassan, Abd-EL-Fattah, M.A and Menofy, S.M (2020) Spectroscopic characterization of preperation, pigment and binding media of archaeological cartonnage from Lisht, Egypt. *SCIENTIFIC CULTURE,* Vol. 6, No. 1, pp. 9-23. DOI: 10.5281/zenodo.3483983.

Al Dabbas, M. , Eisa1, M. Y. and Kadhim, W. H. " Estimation of Gypsum - Calcite percentages using a fourier transform infrared spectrophotometer (FTIR), in Alexandria gypsiferous soil, *Iraqi Journal of Science*, Iraq, Vol 55, No.4B, pp: 1916-1926.

Ambers, J. (2004). Raman analysis of pigments from the Egyptian Old Kingdom. *Journal of Raman Spectroscopy*, 35(8-9), pp. 768-773.

(Apatite) *https://en.wikipedia.org/wiki/Apatite* (accessed on 25-02-2019).

Berry, M. (1999) A study of pigments from a Roman Egyptian shrine, *AICCM Bulletin*, Vol.24, pp.1-9.

Bosch, F., Adelantado, J.V. and Moreno M.C.M. (2002) FTIR quantitative analysis of calcium carbonate (calcite) and silica (quartz) mixtures using the constant ratio method Application to geological samples" *Talanta*, Vol. 58, pp. 811-821.

Bratitsi M, Liritzis I, Alexopoulou A, Makris, D (2019) Visualising underpainted layers via spectroscopic techniques: a brief review of case studies. *SCIENTIFIC CULTURE*, Vol. 5, No. 3, pp. 55-68. DOI:10.5281/zenodo.3340112.

Bracci, S., Caruso, O., Galeotti, M., Iannaccone, R., Magrini, D., Picchi, D., Pinna, D. and Porcinai, S. (2015) Multidisciplinary approach for the study of an Egyptian coffin (late 22nd/ early 25th dynasty): Combining imaging and spectroscopic techniques, *Spectrochimica Acta Part A: Molecular and Bimolecular Spectroscopy*, 145, pp. 511-522. doi: 10.1016/j.saa.2015.02.052. Epub 2015.

Calza, C., Anjos, J., Mendonça de Souza, S., Junior, A. B. and Ricardo, R. (2007) X-Ray microfluorescence analysis of pigments in decorative paintings from sarcophagus cartonage of an Egyptian mummy, *Nuclear Instruments and Methods in Physics Research*, B 263, pp. 249–252.

Calza, C., Freitas, R., Brancaglion A. and Lopes, R. (2011) Analysis of artefacts from Ancient Egyptian using an EDXRF portable system, *International Nuclear Atlantic Conference* - INAC 2011.

Cartwright, C., Spaabæk, L. R. and Svoboda, M. (2011) Portrait mummies from Roman Egypt: ongoing collaborative research on wood identification, *The British Museum Technical Research Bulletin*, Vol.5, pp. 49-58.

Colinart, S. (2001) Analysis of inorganic yellow colour in ancient Egyptian painting. In *Colour and painting in ancient Egypt*, Davies, W.V., (ed.) the British museum press, pp.1-4.

Cosentino, A. (2015) Effects of different binders on technical photography and infrared reflectography of 54 historical pigments, *International Journal of Conservation Science*, Vol.6, Issue 3, pp. 287-298.

Crivellaro, A. and Schweingruber, F. H. (2013) Atlas of Wood, Bark and Pith Anatomy of Eastern Mediterranean Trees and Shrubs with Special Focus on Cyprus, Springer-Verlag, Berlin.

Daines, A. (2008) Egyptian Gardens, *Studia Antiqua*, Vol.6, no.1, p.18.

Darque-Ceretti, E., Felder, E.and Aucouturier, M. (2011) Foil and leaf gilding on cultural artefacts: forming and adhesion, *Revista Matéria* 16(1), pp. 540–559. Doi: 10.1590/S1517-70762011000100002.

David, A. R., Edwards, H.G.M. and Farwell, D.W., and Defaria, D.L.A. (2001) Raman spectroscopic analysis of ancient Egyptian pigments, *Archaeometry*, 43, 4, pp. 461-473.

Dawson, J., Marchant, J., Von aderkas, E., Kartwright, C. and Stacey, R. (2016) *Egyptian coffins: Materials, Construction and deterioration, Death on the Nile: Uncovering the afterlife of ancient Egypt* (foreword by T. Knox) the Fitzwilliam Museum, Cambridge, pp.75-112.

Derrick, M, Stulik D. and Landry, J. (1999) *Scientific Tools for Conservation: Infrared Spectroscopy in Conservation Science,* The Getty Conservation Institute, Los Angeles, USA, p. 150.

Donaldson, L.A. (2009) Analysis of fifers using microscopy: Fundamentals and manufactured polymer fibres, in *Handbook of textile fibre structure*, S. J. Eichhorn, J.W.S. Hearle, M. Jaffe and T. Kikutani (ed.). Woodhead Publishing Limited, p.121.

Dyer, J, O'Connell, E.R and Simpson, A (2014) Polychromy in Roman Egypt: A study of a limestone sculpture of the Egyptian god Horus, *Technical Research Bulletin, The British Museum*, Vol. 8, pp. 93-103.

Florian, M.E. (1990) Identification of Plant and Animal Materials in Artefacts, In *The conservation of artifacts made from plant materials*, Florian, M. E., Kronkright, D.P. and Norton, R. E. (ed.), The Getty Conservation Institute, p.49.

Gale, R., Gasson P. And Hepper N. (2000) wood [Botany]. In *Ancient Egyptian materials and technology*, Shaw, I. and Nicholson, P. (ed.), the American University in Cairo press, pp.334-352.

Garcia –Moreno, R., Hocquet, F., Mathis, F., Van Elslande, E., Strivay, D. And Vandenabeele, P. (2013) Archaeometry research on wall painting in the tomb chapel of menna, The Tomb Chapel of Menna (TT69). In: *The Art, Culture, and Science of Painting in an Egyptian Tomb V,* M. Hartwig (ed.), An American Research Centre in Egypt.

Goltz, D., Mcclelland, J., Schellenberg, A., Attas, M., Cloutis, E. and Collins, C. (2003) Spectroscopic Studies on the Darkening of Lead White, *Society for Applied Spectroscopy*, Vol. 5, pp. 1393-1398.

Grant, M.S. (2000) The use of ultraviolet induced visible-fluorescence in the examination of museum objects, Part II, *Conserve O Gram - National Park Service*, Vol.1, pp. 1 - 3.

Green, L. (2001) Colour transformations of ancient Egyptian pigments, In: *Colour and painting in ancient Egypt*, Davies, W.V., (ed.) the British Museum Press, pp. 43-48.

Hatchfield, P. and Newman, R. (1991) Ancient Egyptian gilding methods. In: *Gilded Wood: Conservation and History*, D. Bigelow (ed.), Sound View Press, Madison CT, pp.27–47.

Heywood, A. (2001) The use of huntite as a white pigment in ancient Egypt, In *Colour and painting in ancient Egypt*, Davies, W.V., (ed.) the British Museum Press, pp. 5-9.

Hoadley, R. B. (1990) Identifying Wood, *the Taunton Press*.

Hradil, D., Grygar, T., Hradilova´ J. and Bezdic˘ka, P. (2003) Clay and iron oxide pigments in the history of painting, *Applied Clay Science* , Vol.22, pp. 223–236.

Hühnerfuβ, K., Bohlen, A. and Kurth, D. (2006) Characterization of pigments and colors used in ancient Egyptian boat models, *Spectrochimica Acta Part B(61): Molecular and Bimolecular Spectroscopy 145*, pp. 1224-1228.

IAWA Committee (1989) List of microscopic features for hardwood identification. *IAWA Bulletin n.s.*, Vol. 10 (3).

(Identification of Carpet beetles) *https://www.agric.wa.gov.au/pest-insects/identifying-and-controlling-clothes-moths-carpet-beetles-and-silver* (accessed on 12-02-2019).

(Identification of museum pests) *http://museumpests.net/identification/* (accessed on 12-02-2019).

James, T.G.H. (1972) Gold Technology in Ancient Egypt, mastery of metal working methods, *Gold Bulletin*. Vol.2 (5), pp. 35 –38.

Korenberg, C. (2008) The photo-ageing behaviour of selected watercolour paints under anoxic conditions, *technical research bulletin*, the British museum, Vol. 2, pp. 49-57.

Lee, L. and Quirke, S. (2000) Painting materials. In: *Ancient Egyptian materials and technology*, Shaw, I. and Nicholson, P. (ed.), the American university in Cairo press, pp.104-119.

Lucas, A. and Harris, J.R. (1989) Ancient Egyptian Materials and Industries, *Histories and Mysterious of man*, London, p.447, 344.

Mahmoud H. M. (2014) Investigations by Raman microscopy, ESEM and FTIR-ATR of wall paintings from Qasr el-Ghuieta temple, Kharga Oasis, Egypt, *Heritage Science*, Vol.2, paper no. 18.

Mahmoud, H. M., Kantiranis, N. and Stratis, J. (2012) a Technical Characterization of Roman Plasters, Luxor Temple, upper Egypt. In *Mediterranean Archaeology and Archaeometry*, Vol. 12, No.2, pp. 81-93.

Mazzocchin, G.A., Agnoli, F., Mazzocchin, S. and Colpo, I. (2003) Analysis of pigments from Roman wall paintings found in Vicenza, *Talanta*, Vol. 61, pp. 565-572.

Mazzocchin, G.A., Agnoli, F. and Colpo, I. (2003) Investigation of roman age pigments found on pottery fragments, *Analytica Chimica Acta* Vol.478, pp.147–161.

McCarthy, B. (2001) Technical analysis of reds and yellows in the tomb of Suemniwet, Theban tomb 92. In W. V. Davies (ed.) *Colour and Painting in Ancient Egypt*, London,British Museum Press, pp. 17–21.

Medhat, A Abdrabou, A, Kamal, H.M (2018) Analytical study and conservation processes of Tutankhamen decorated stick: a case study. *SCIENTIFIC CULTURE*, Vol. 4, No 1, pp. 93-100 DOI: 10.5281/zenodo.1048249.

National park service (2008) Identifying Museum Insect Pest Damage, *Conserve o Gram*, No.3/11, pp. 1-7.

Pagès-Camagna, S. and Guichard, H. (2010) Egyptian colours and pigments in French collections: 3o years of physicochemical analyses on 3oo objects, *Decorated surfaces on ancient Egyptian objects technology, deterioration and conservation*, Dawson, J., Rozeik, C., and Wright, M.M. (ed.), Proceedings of a conference held in Cambridge, UK, in association with The Fitzwilliam Museum, *Cambridge Research Institute of Conservation*, pp.25-31.

Passmore, E., Ambers , J., Higgitt, C., Ward, C., Wills, B., Simpson, S.J. and Cartwright, C. (2012) Hidden, looted, saved: The scientific research and conservation of a group of Begram Ivories from the National Museum of Afghanistan, *The British Museum Technical Research Bulletin,* Vol.6, pp. 33-46.

Peacock, E.R. (1993) *Adult and larvae of hide, larder and carpet beetles and their relatives (Coleoptera: Dermestidae)*, *Royal Entomological Society of London,* Vol.5, part 3, pp. 40-42.

(Pigments Catalogue) *http://www.webexhibits.org/pigments/intro/pigments.html* (accessed 2019-02-15).

(Raking light) *https://www.nationalgallery.org.uk/paintings/glossary/raking-light* (accessed 2019-01-17).

Rifai, M. and El Hadidi, N. (2010) Investigation and analysis of three gilded wood samples from the tomb of Tutankhamen. In: *Decorated Surfaces on Ancient Egyptian Objects Technology, Deterioration and Conservation*, J. Dawson, C. Rozeik, and M.M. Wright (ed.), Proceedings of a conference held in Cambridge, UK, in association with The Fitzwilliam Museum*, Cambridge Research Institute of Conservation*, pp.16-24.

Scott, D., Dodd, L.S., Furihata, J., Tanimoto, S., Keeney, J., Schilling, M.R., and Cowan, E. (2004) An Ancient Egyptian Cartonnage Broad Collar: Technical Examination of Pigments and Binding Media, *Studies in Conservation*, Vol. 49, No. 3, pp. 177-192.

Stuart, B.H. (2007) Analytical Techniques in Materials Conservation, John Wiley, England, p.73.

(Tamarix sp.), in *The inside Wood Database*, *http://insidewood.lib.ncsu.edu/results?25* (accessed 2019-01-17).

(The Identification of Natural Fibres - Canadian Conservation Institute (CCI) Notes 13_18 – Canada) *https://www.canada.ca/en/conservation-institute/services/conservation-preservation-publications/canadian-conservation-institute-notes/identification-natural-fibres.html* (accessed on 15-02-2019).

Uda, M., Sassa, S., Yoshimura, S., Kondo, J., Nakamura, M., Ban, Y. and Adachi, H. (2000) Yellow, red and blue pigments from ancient Egyptian palace painted walls, *Nuclear Instruments and Methods in Physics Research*, B 161-163, pp. 758-761.

Verri , G., Clementi, C., Comelli, D., Cather, S. and Pique, F.(2008) Correction of Ultraviolet-Induced Fluorescence Spectra for the Examination of Polychromy, *Applied Spectroscopy*, Vol.62(12), pp. 1295-1302.

Verri, G., Opper, T. and Deviese, T. (2010) The 'Treu Head': A case study in Roman sculptural polychromy, *Technical Research Bulletin*, Vol.4, pp. 39-54.

Verri , G., Saunders, D., Ambers, J. and Sweek , T. (2010) Digital mapping of Egyptian blue: Conservation implications, *Studies in Conservation*, Vol.55(Sup. 2), pp. 220-224.

Verri, G., Gleba , M., Swaddling, J., Long, T., Ambers, J. and Munden, T. (2014) Etruscan women's clothing and its decoration: the polychrome gypsum statue from the 'Isis Tomb' at Vulci, *Technical Research Bulletin*, Vol.8, 2014, pp. 59-71.

Waltom, M. S. And Trentelman, K. (2009) Romano-Egyptian red lead pigment: A subsidiary commodity of Spanish silver mining and refinement, *Archaeometry* 51, 5 (2009) 845–860.

Welcomme, E., Walter, P., van elslande, E. and Tsoucaris, G. (2006) Investigation of white pigments used as make-up during the Greco-Roman period, *Materials Science & Processing Applied Physics*, pp. 551–556.

Wei, Y., Jun-Cheng, L., Shu-Mei, W., Sheng-Wang, L. & Jiang-Yong Y. (2016) The FTIR fingerprint of gypsum fibrosum, *Acta Medica Mediterranea*, Vol.32, pp. 607-611.